WILEY | Hindawi

Research Article

Mesoparameter Calibration and Macro-Mesoparameter Correlation of Tailing Sand

Changbo Du [iD],[1] Lidong Liang [iD],[1] Hailong Cheng [iD],[2] Fu Yi [iD],[3] and Ben Niu [iD][1]

[1]*College of Civil Engineering, Liaoning Technical University, Fuxin, Liaoning Province 123000, China*
[2]*Changchun High New Technology Building Development, Inc., Changchun 130000, China*
[3]*College of Architecture and Transportation, Liaoning Technical University, Fuxin, Liaoning Province 123000, China*

Correspondence should be addressed to Changbo Du; duchangbo2839@163.com

The aim of this study was to explore the correlation between mesoparameters (normal stiffness k_n, tangential stiffness k_s, and friction coefficient fric) and macromechanical parameters (cohesion, internal friction angle, and peak principal stress as well as its corresponding stress variables) of the particle flow code in 3-dimension (PFC3D) built-in linear contact model, which is suitable for simulating cohesionless materials that are similar to tailing sand. A triaxial test model was established using PFC3D, and nonspherical particles were developed by the clump command. Several numerical triaxial tests were performed under different confining pressures and mesoparameters. The results showed that the linear contact model is effective in simulating sandy soil, and the corresponding gradation of particles should be given. No one-to-one correspondence was found between the macromechanical parameters and the mesoparameters. Each macromechanical parameter was most affected by a certain mesoparameter, and the degree of influence was much greater than that of the other mesoparameters. The macro- and mesoparameters were strongly correlated. The stiffness ratio (k_n/k_s) mainly affected the cohesion value, the friction coefficient of fillers (pebble-fric) mainly affected the internal friction angle and the peak principal stress, the normal stiffness (k_n) of particles mainly affected the strain corresponding to the peak principal stress, and the influence of the side wall friction coefficient (wall-fric) was not the strongest but was non-negligible. The microparameter calibration of the contact model can follow the order of parameter adjustment proposed in this study, which can facilitate and enhance the accuracy of the parameter calibration process of the linear contact model.

1. Introduction

Particle flow code in 3 dimensions (PFC3D) simulation drawing tests have been used for investigating the interface mechanical properties of geosynthetics reinforced tailing sand. The accuracy of PFC numerical simulations is directly determined by the selection accuracy of the mesoparameters of the contact models [1]. Currently, the mesoparameters are selected and compared by trial and error: researchers first assume a set of mesoparameters and then continuously adjust the parameters until the macromechanical properties of the model are similar to those of laboratory test results. This process is usually time-consuming and difficult to use in obtaining the desired calibration results.

Different mesoparameters have been selected as the basis for parameter calibration in various studies [2–6]. Huang et al. [7] first used a bond model to investigate the proportional rule of macro- and mesomechanical properties of PFC2D samples. Potyondy and Cundall [3] used a parallel bond model to simulate the characteristics of rock mechanics. The relationships between the macro- and mesoparameters of two- and three-dimensional models were deduced from comparative analyses. Zhang et al. [8] compared numerical simulations with laboratory test results and found that the proposed cross-scale constitutive model can not only quantitatively describe the effect of immersion weakening on soil mechanical behavior at the macroscale but can also adequately reflect the bond dissolution at the mesoscale. Renzo and Maio

[9] proposed the ratio of initial tangential stiffness to normal stiffness by investigating the mechanical properties of materials. Hentz et al. [10] used the discrete element method to study the mechanical properties of concrete. They used the least squares principle to establish the relationship between macro elastic constants and mesocontact stiffness. Yang et al. [11] used rock samples to investigate the relationship between particle mesoparameters and elastic parameters, such as the modulus of elasticity and Poisson's ratio, as well as the uniaxial compressive strength in a parallel bonding model. Yoon [12] used the central composite design to calibrate the mesoparameters of the contact bond model and studied the linear correlation between the mesoparameters and macromechanical properties of the elastic modulus, Poisson's ratio, and uniaxial compressive strength of rock. Cong et al. [13] used PFC2D to simulate the mechanical properties of marble using the parallel bond contact model. They discussed the relationship between the mesoparameters of the contact model, elastic modulus, Poisson's ratio, peak stress, and failure mode. Zhou et al. [14] studied the influence of the stiffness ratio, porosity, and confining pressure of the linear contact model on the initial elastic modulus and Poisson's ratio using a PFC3D simulation indoor triaxial test. They established a functional relationship between the macro- and mesoparameters. To investigate the mechanical properties of cohesion soils, Xu et al. [15] used PFC2D to simulate biaxial tests performed by the contact bond model. They investigated the relationships between the mesoparameters of the contact model and the shear strength parameters, cohesion, and internal friction angle.

Currently, researchers mostly focus on the correlation between the mesoparameters of the bond model (i.e., normal bond stiffness, tangential bond stiffness, normal bond strength, and tangential bond strength) and the macromechanical parameters (i.e., elastic modulus, Poisson's ratio, and compressive strength). The bond model is mostly used to simulate the viscous comparison of rock and concrete. For strong materials, few studies have been conducted on linear contact models for soils with low cohesion, and no report exists on the relationship between the mesoparameters of linear models and the shear strength parameters of soils with low cohesion.

In this study, PFC3D was used to establish a triaxial compression test model, and a series of numerical triaxial tests were performed under single-factor change conditions. We investigated the relationships between the mesoparameters (normal stiffness k_n, tangential stiffness k_s, and friction coefficient fric) and macromechanical parameters (cohesion c, internal friction angle φ, peak principal stress, and axial strain) of tailing sand. The peak value of the principal stress and its corresponding axial strain were controlled, and the deviation stress–axial strain curve was similar to that obtained from laboratory tests; the calibration result was verified by shear strength parameters.

2. Establishment of Triaxial Test Model for Tailing Sand

The triaxial test model built in this study is similar to that used by Huang et al. [16]. The prescribed velocity is applied
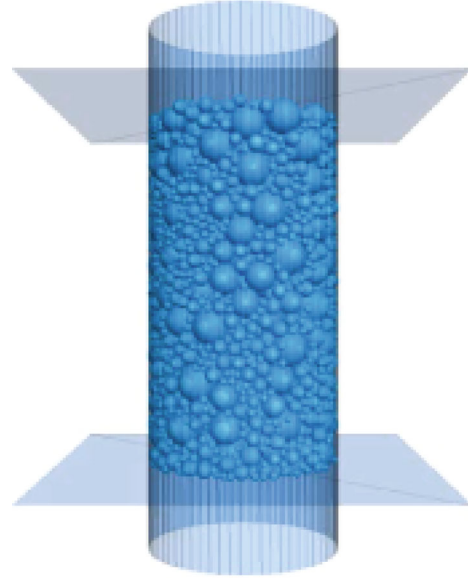

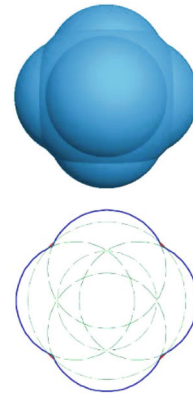FIGURE 1: Triaxial test model.

FIGURE 2: Particles and their profiles.

to the upper and lower planar walls in our model to simulate compression, and confining pressure is applied to the surrounding circular walls. Figure 1 shows the test model; the specimen was 8 cm in height and 4 cm in diameter. The modeling process was as follows:

(1) The cylindrical, upper, and lower planar walls were generated

(2) In the space enclosed by the walls, fillers were formed according to the porosity and gradation under different compactness levels. In the linear contact model, when the normal stiffness of the wall was not less than the normal stiffness of the particles, the filler and wall were endowed with a smaller tangential stiffness and friction coefficient. The overlap was eliminated and unbalanced forces reduced; reducing the parameters facilitated the rapid and uniform distribution of the particles in reaching the initial equilibrium
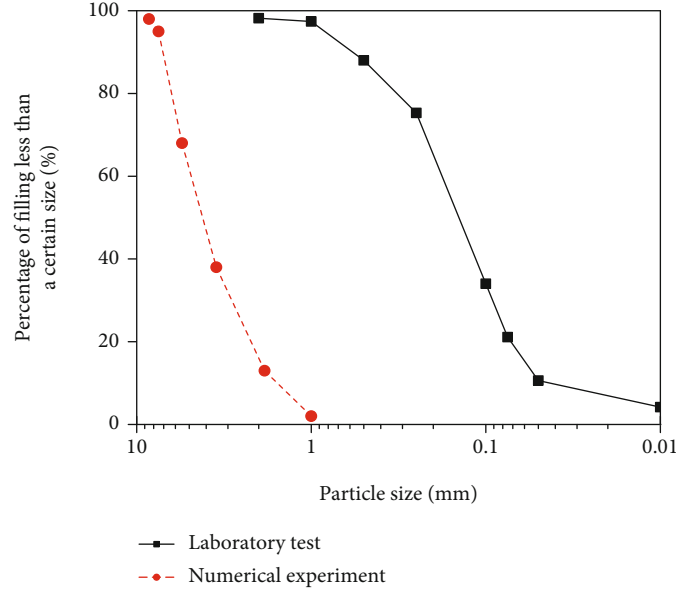
FIGURE 3: Gradation curve of numerical and indoor tests.

TABLE 1: Preliminary mesoparameter assumption of tailing sand and wall.

Category	k_n (N/m)	k_s (N/m)	Fric	ρ (kg/m^3)
Wall	1.0×10^5	1.0×10^5	0.4	/
Clump	1.0×10^6	1.0×10^6	0.5	1600

Note: k_n is the normal stiffness, k_s is the tangential stiffness, fric is the friction coefficient, ρ is density, wall is the sidewall, and clump is the filler particles.

(3) To change the normal stiffness of the cylindrical wall, one-tenth of the normal particle stiffness was used for simulating the flexible boundary of the indoor triaxial test and for changing the parameters to their predetermined values. Servo control was applied to the cylindrical, upper, and lower walls to enable the model reach the initial state under the preset confining pressure

(4) The servo control of the upper and lower walls was cancelled, and the compression speed was applied, thereby commencing the test. The servo control of the upper and lower walls was then cancelled, the compression speed was applied, and the test commenced. To prevent impact effect, the upper and lower walls were accelerated step-by-step to a predetermined compression speed of 0.03 mm/min, and the test was stopped when a certain amount of compression was attained after the peak value

3. Hypothesis of Tailing Parameters and Gradation Effect on Test Results

The size of the tailing sand should be enlarged properly when establishing the numerical test model because the sand particles are small. After enlargement, the ratio of the particle size to model size differs from that of the original particle size to laboratory test size. It is unnecessary to obtain the exact shape of the tailing sand under this condition. An important task is the determination of the particle and model sizes for the PFC numerical simulation test. Simulation results are typically inaccurate when the particle size is less than 2,000 units [17]. Similar macromechanical properties can be obtained by simulating tailing sand using spherical particles, which are necessary for improving the mesoparameters but face numerous drawbacks [18, 19]. The nonspherical particles are typically developed by the clump command to improve simulation accuracy. Most nonspherical particles used in previous studies were not symmetrical in space, which caused fluctuations in the stress–strain curve [16]. Figure 2 shows the nonspherical particle used in this study. The particle consists of a sphere with a middle radius of 2 mm and a sphere with a radius of 1.5 mm symmetrically distributed in space. The model is characterized by the good spatial isotropy of the particles, which is crucial for the smooth transitioning of stress–strain curves and for overcoming the drawbacks of the over-rotation of pure circular particles. Because of the gradation in the inherent particle composition of sand, the simulated tailings gradation used in this study is similar to that used in a previous study [20]. The values of the coefficient of uniformity $C_U = 4 < 5$ and coefficient of curvature $C_C = 1$ obtained from the laboratory screening test showed poor sand gradation. In the numerical experiments, the particle size was adjusted to keep C_U and C_C constant to avoid a deviation from fine gradation The adjustment was performed to maximize the simulation of the real tight contact between sand particles. Figure 3 shows the gradation curve. The adjusted values were as follows: effective particle size $d_{10} = 1.68$ mm, median particle size $d_{30} = 3.21$ mm, restricted particle size $d_{60} = 6.68$ mm, $C_U = 3.976$, and C_C
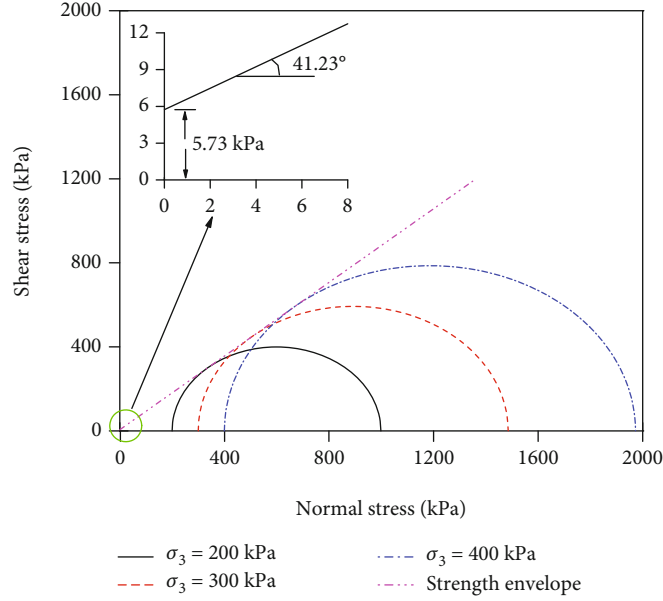
Figure 4: Mohr's circle under preliminary mesoparameters.

Table 2: Summary of results of three working conditions.

Parameter	Working condition I	Working condition II	Working condition III
	Peak normal stress σ_1 (kPa)		
$\sigma_3 = 200$ kPa	998.8	785.3	1029.1
$\sigma_3 = 300$ kPa	1485.5	1172.2	1537.8
$\sigma_3 = 400$ kPa	1972.5	1559.9	2058.1
Cohesion c (kPa)	5.73	2.7	1.99
Internal friction angle φ (°)	41.23	36.13	42.23

= 0.918. Hence, the tailings were poorly graded sand, and the values of C_U and C_C were close to those of the laboratory test results.

Table 1 presents the preliminary mesoparameters of tailings that were selected by adjusting the parameters of the model for trial calculation, and Figure 4 shows the Mohr's circle and strength envelope. The results are similar to the interface strength parameters (cohesion of 4.7 kPa and internal friction angle of 32.89°) measured by a previous indoor triaxial test [20], and the errors between both results were 17.98% and 20.23%, respectively.

According to the mesoparameters presented in Table 1, the effects of the particle shape and gradation were investigated by simulating three working conditions: non-spherical particles with gradation (working condition I), spherical particles with gradation (working condition II), and nonspherical particles without gradation (working condition III). The average particle size ($d_{50} = 0.55$ mm) without a consideration of gradation was the same as the average particle size with a consideration of gradation. The nonspherical particles used in this study fully reflect the shear strength caused by angular characteristics under small confining pressure conditions. Hence, the peak principal stress

was generally smaller under a confining pressure of 100 kPa while a more accurate strength envelope was obtained under confining pressures of 200 kPa, 300 kPa, and 400 kPa. The results of three working conditions under the same mesoparameters are presented in Table 2, and the deviation stress–axial strain is shown in Figure 5.

Figure 5 illustrates a comparison of the results of working conditions I and II: the peak deviating stress of the simulated nonspherical particles under the three-stage confining pressure conditions was higher than that of the spherical particles, and the cohesion and internal friction angle also increased. The shapes of the stress–strain curves are similar, and both curves show strain softening characteristics. The nonspherical particles in the numerical simulation were more consistent with the actual situation while contributing to the accuracy of the test results. The results of working conditions I and III under the condition of considering particle gradation were compared: the peak deviating stress under the three-stage confining pressure conditions differed substantially from that under the condition of not considering gradation. The peak deviating stress of the test results under condition I increased considerably, showing strain-softening characteristics; the peak deviating stress of the test results under condition II did not increase substantially, showing strain-hardening characteristics. To obtain the same macromechanical properties, it is necessary to set higher mesoparameters when ignoring particle gradation than when considering it. Thus, considering the particle size distribution in the numerical simulation increased the contact proximity between the particles and strengthened the interlocking effect. The results showed that the friction cohesion increased while the stress–strain curve was smoother, which is more consistent with the laboratory test results. Therefore, the results of the indoor test were more consistent with those obtained under condition I. In the PFC3D numerical simulation, the effect of gradation and particle
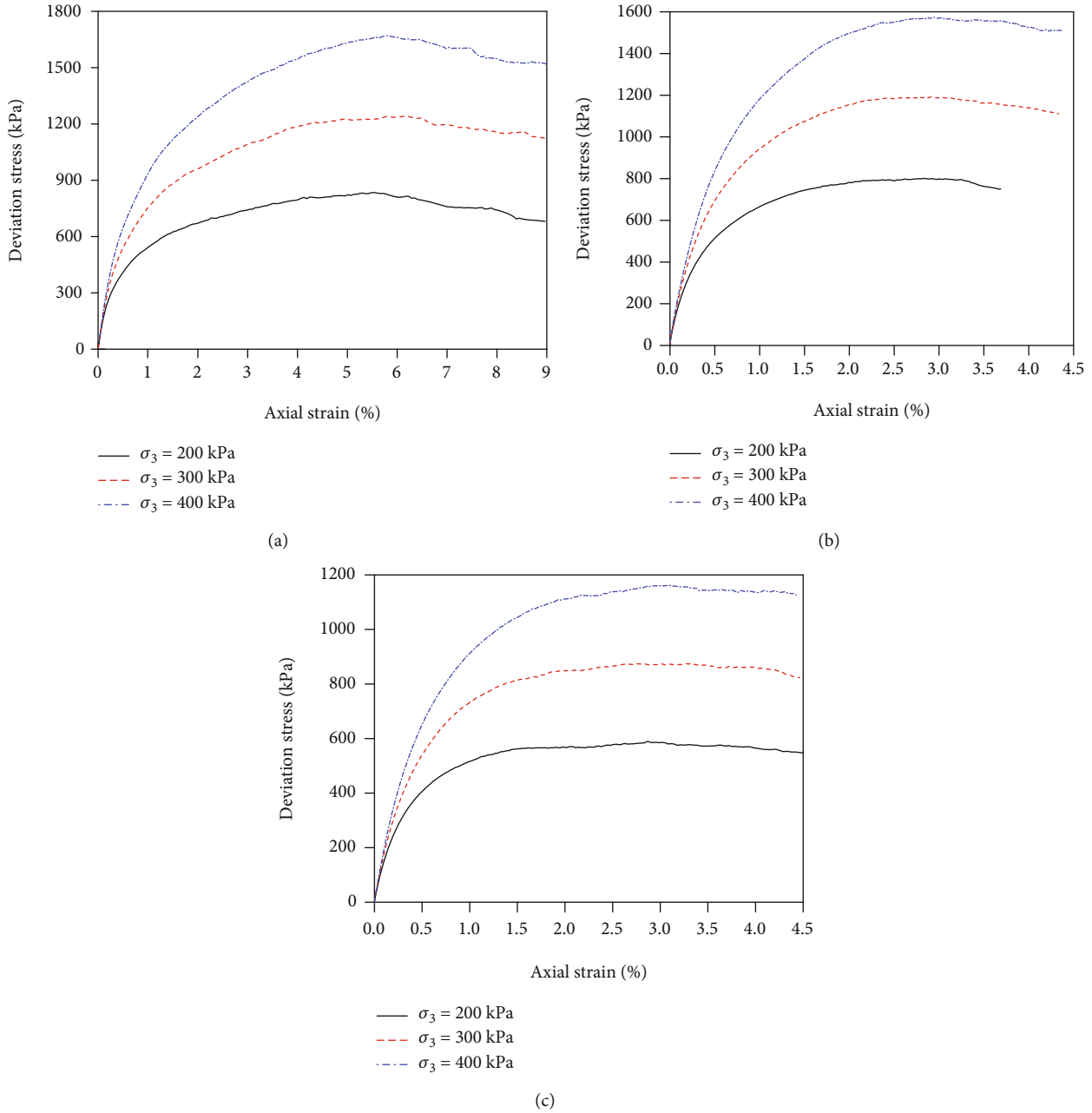
(a)

(b)

(c)

FIGURE 5: Deviation stress-axial strain curve of triaxial test: (a) non-spherical particles with gradation (working condition I); (b) spherical particles with gradation (working condition II); and (c) non-spherical particles without gradation (working condition III).

shape on the test results was closer to that of the indoor test results.

4. Correlation Analysis of Macro-Mesoparameters Used to Simulate Tailings

4.1. Influence of Normal Stiffness (k_n) on Macromechanical Parameters. According to the preliminary selected meso-parameters, tests were performed on 11 groups with the normal particle stiffness (k_n) ranging from 7.0×10^5 to 4.0×10^6. The results of the linear fitting test, illustrated in Figure 6, were obtained to determine the shear mechanical parameters of the interface.

Figures 6(a) and 6(b) show an increase in k_n and a decrease in the cohesion and internal friction angles; the change trends were similar. When the stiffness was less than 1.75×10^6 N/m, the cohesion and internal friction angles decreased rapidly while k_n increased. As k_n increased further, both cohesion and internal friction decreased slowly, which was more evident for cohesion. When k_n increased from 7.0×10^5 N/m to 4.0×10^6 N/m, the cohesion decreased from 8.52 kPa to 1.18 kPa, a total decrease of 86.15%, and the internal friction angle decreased from 41.36° to 40.37°, a total decrease of 2.39%.

Figure 6(c) shows similarities in the effect of the k_n of the particles on the peak principal stress under the three
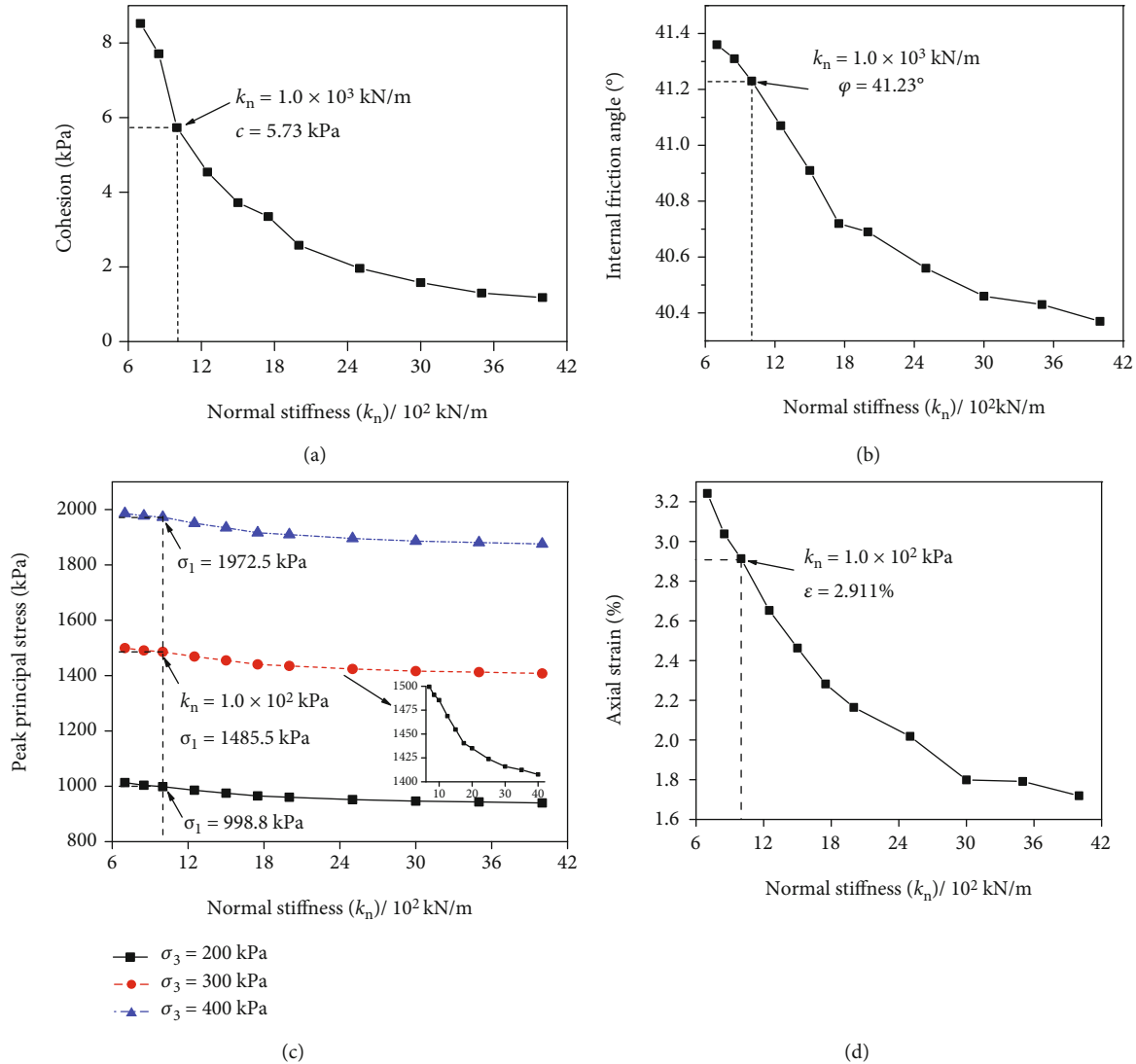
(a)

(b)

(c)

(d)

FIGURE 6: Influence of k_n on macromechanical parameters: (a) cohesion, (b) internal friction angle, (c) peak principal stress, and (d) axial strain.

confining pressure conditions. The peak principal stress decreased with an increase in k_n, but the decreasing rate gradually slowed down. At the confining pressure of 300 kPa, while the value of k_n increased from 7.0×10^5 N/m to 4.0×10^6 N/m, the peak principal stress decreased from 1499.43 kPa to 1407.99 kPa, which is approximately a 6.10% decrease.

Figure 6(d) shows that, under the confining pressure of 300 kPa, the axial strain corresponding to the peak principal stress decreased with an increase in k_n, and the reduction speed also decreased. The axial strain decreased from 3.24% to 1.72%, a total decrease of 46.91%, because an increase in k_n resulted in a decrease in tangential stiffness (k_s). The allowable overlap between particles decreased continuously, and the displacement mainly stemmed from the dislocation of the filler particles, which attained the peak principal stress when the displacement was small.

4.2. Influence of Stiffness Ratio (k_n/k_s) on Macromechanical Parameters. According to the preliminary mesoparameters,

the stiffness ratio (k_n/k_s) varied by changing only the tangential stiffness value k_s. Tests were performed on 12 groups with k_n/k_s ranging from 1.0 to 10.0. The results of the linear fitting tests were obtained to determine the shear mechanical parameters of the interface, as shown in Figure 7.

Figures 7(a) and 7(b) show that the cohesion increased with a corresponding increase in k_n/k_s. When k_n/k_s was between 1 and 3, the cohesion increased linearly with k_n/k_s. When k_n/k_s was between 3 and 12, the increasing rate of the cohesion slowed down gradually. The internal friction angle decreased with an increase in k_n/k_s. When k_n/k_s was between 1 and 3, the linear relationship between the decrease in the internal friction angle and increase in k_n/k_s was maintained, and when k_n/k_s was between 3 and 12, the decreasing rate of the internal friction angle decreased gradually. As k_n/k_s increased from 1 to 12, the cohesion increased from 5.73 kPa to 20.16 kPa, which is a total increase of 251.83%, and the internal friction angle decreased from 41.23° to 38.59°, which is a total decrease of 6.40%.
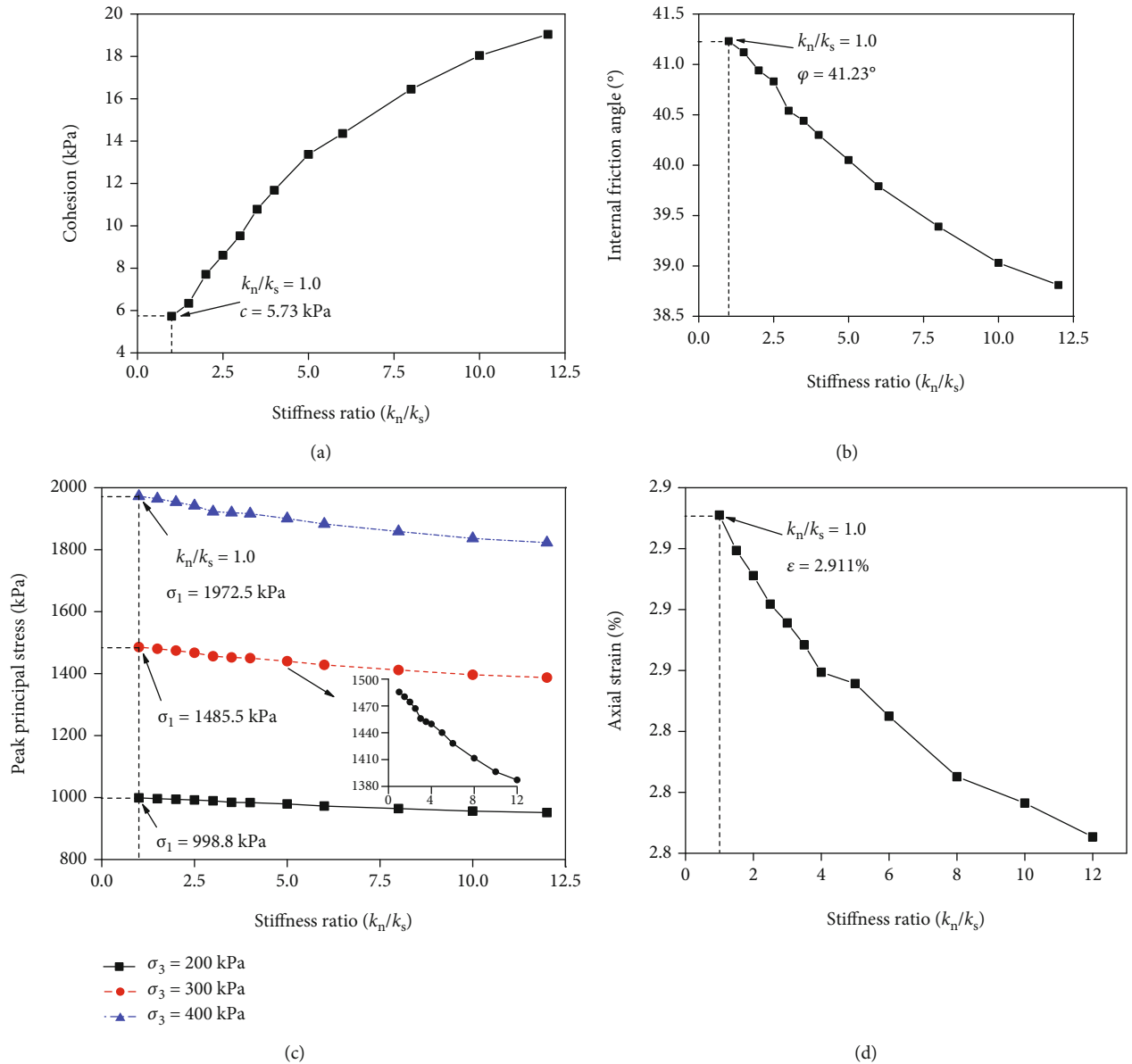
(a)

(b)

(c)

(d)

Figure 7: Influence of k_n/k_s on macromechanical parameters: (a) cohesion, (b) internal friction angle, (c) peak principal stress, and (d) axial strain.

Figure 7(c) shows that the principal stress decreased as k_n/k_s increased under the three confining conditions, and the three changes were almost parallel. The principal stress decreased linearly as k_n/k_s increased from 1 and 12. When k_n/k_s exceeded 3, the rate of change of the principal stress decreased gradually as k_n/k_s increased.

Figure 7(d) shows that the strain corresponding to the peak principal stress decreased with an increase in k_n/k_s at the confining pressure of 300 kPa, and the rate of change decreased gradually. The peak principal stress decreased from 1485.5 kPa to 1387.2 kPa by 6.62%, and the axial strain decreased from 2.91% to 2.81% by 3.44%. The results obtained by reducing the tangential stiffness k_s to increase k_n/k_s were consistent with those obtained by increasing the normal stiffness, as described in the previous section, demonstrating the accuracy of the results.

4.3. Influence of Friction Coefficient (fric) on Macromechanical Parameters

(1) Friction coefficient of fillers (pebble-fric)

Studies have mainly focused on the influence of the friction coefficient of fillers (pebble-fric) on the shear resistance of fillers, and the friction coefficient of the side wall (wall-fric) has been neglected or set to zero, unlike in the indoor test. pebble-fric and wall-fric were changed separately to investigate their effects on shear strength parameters. pebble-fric was changed from 0.4 to 3.0 according to the preliminary selected model parameters. Eleven tests were performed, and the results are presented in Figure 8.

Figures 8(a) and 8(b) show that as pebble-fric increased, the cohesion first increased and then decreased. The
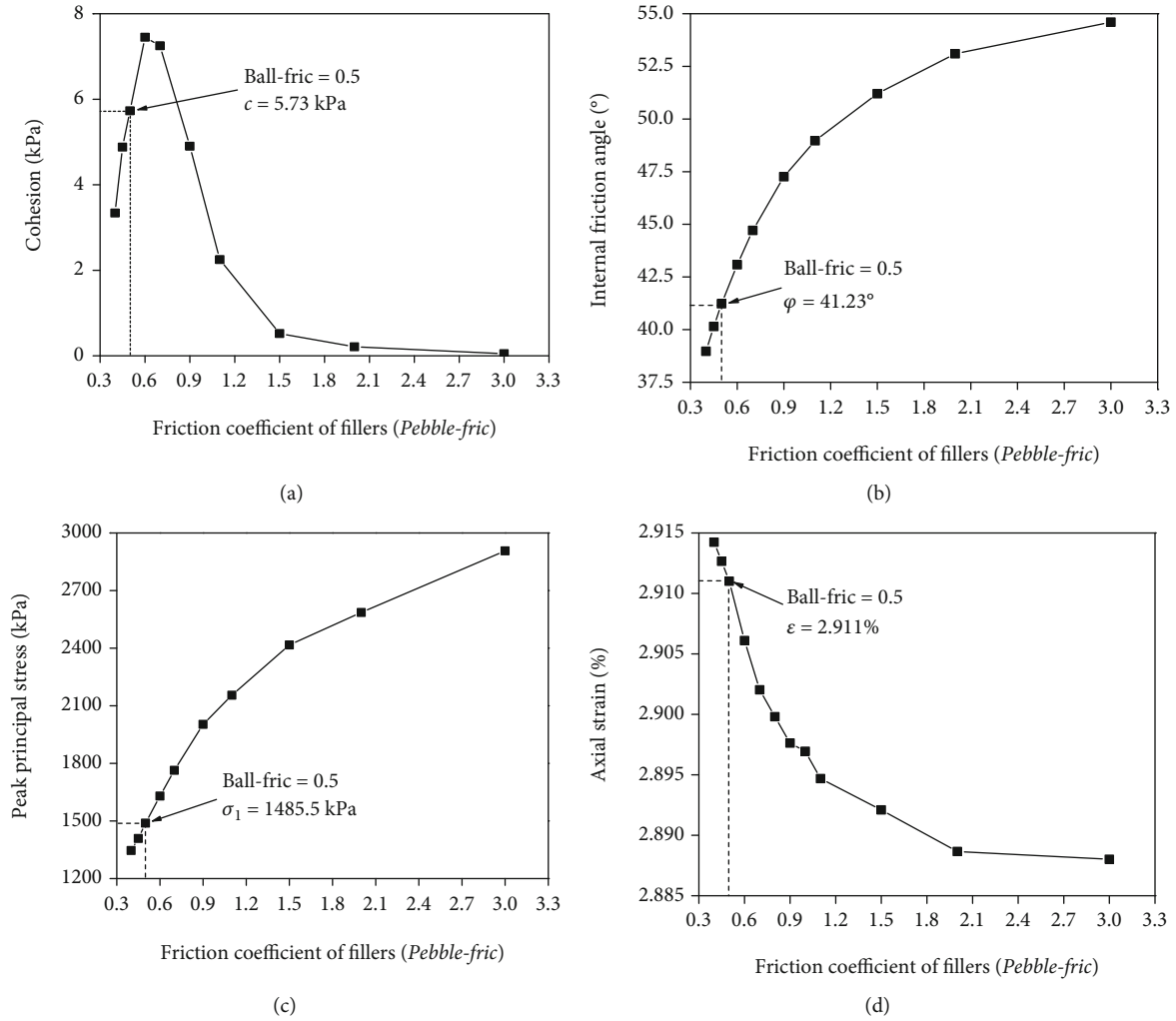
(a)

(b)

(c)

(d)

FIGURE 8: Influence of pebble-fric on macromechanical parameters: (a) cohesion, (b) internal friction angle, (c) peak principal stress, and (d) axial strain.

cohesion reached its maximum when the friction coefficient was approximately 0.6, decreased rapidly from 0.8 to 1.5, and then slowed down gradually. The internal friction angle increased gradually with an increase in pebble-fric; beyond a friction coefficient of 1.5, the rate of increase gradually slowed down. Before pebble-fric reached 1.0, the rate increased almost linearly. When pebble-fric increased beyond 1.0, the rate of increase gradually slowed down. Here, the maximum and minimum cohesion forces were 7.45 kPa and 0.05 kPa, respectively, and the range of variation was 99.33%. The internal friction angle increased from 38.97° to 54.60°, with a total increase of 40.11%. The ball friction coefficient had an influence on the maximum principal stress and corresponding axial strain, and the law of variation under each confining pressure was similar to that described in Sections 4.1 and 4.2.

Figure 8(c) shows that the peak principal stress increased with increasing pebble-fric. When pebble-fric was less than 1.0, the increase in the peak principal stress was nearly linear with respect to the increase in pebble-fric. When pebble-fric exceeded 1.0, the rate of increase gradually slowed down.

As shown in Figure 8(d), for a confining pressure of 300 kPa, the axial strain corresponding to the peak principal stress decreased rapidly with an increase in pebble-fric, and the reduction rate decreased rapidly. The peak principal stress increased from 1,346.1 kPa to 2,907.3 kPa, an increase of 115.97%; the axial strain decreased from 2.91% to 2.89%, a decrease of 0.69%.

(2) Friction coefficient of side wall (wall-fric)

According to the selected mesoparameters, only the friction coefficient of the side wall (wall-fric) was varied to study the influence of wall-fric on shear strength parameters. Eight tests were performed with k_s set at 6.7×10^5 N/m and 1.0×10^6 N/m and with wall-fric set at 0.2, 0.3, 0.4, and 0.5. The maximum wall-fric was 0.5 as the side wall friction is typically reduced by specific methods in the actual test; the side wall friction was less than the internal friction angle of the filler. The selected pebble-fric was 0.5, and the maximum wall-fric was 0.5. The results are illustrated in Figure 9.

Figures 9 (a) and 9(b) show that wall-fric had an influence on the numerical test results and could not be
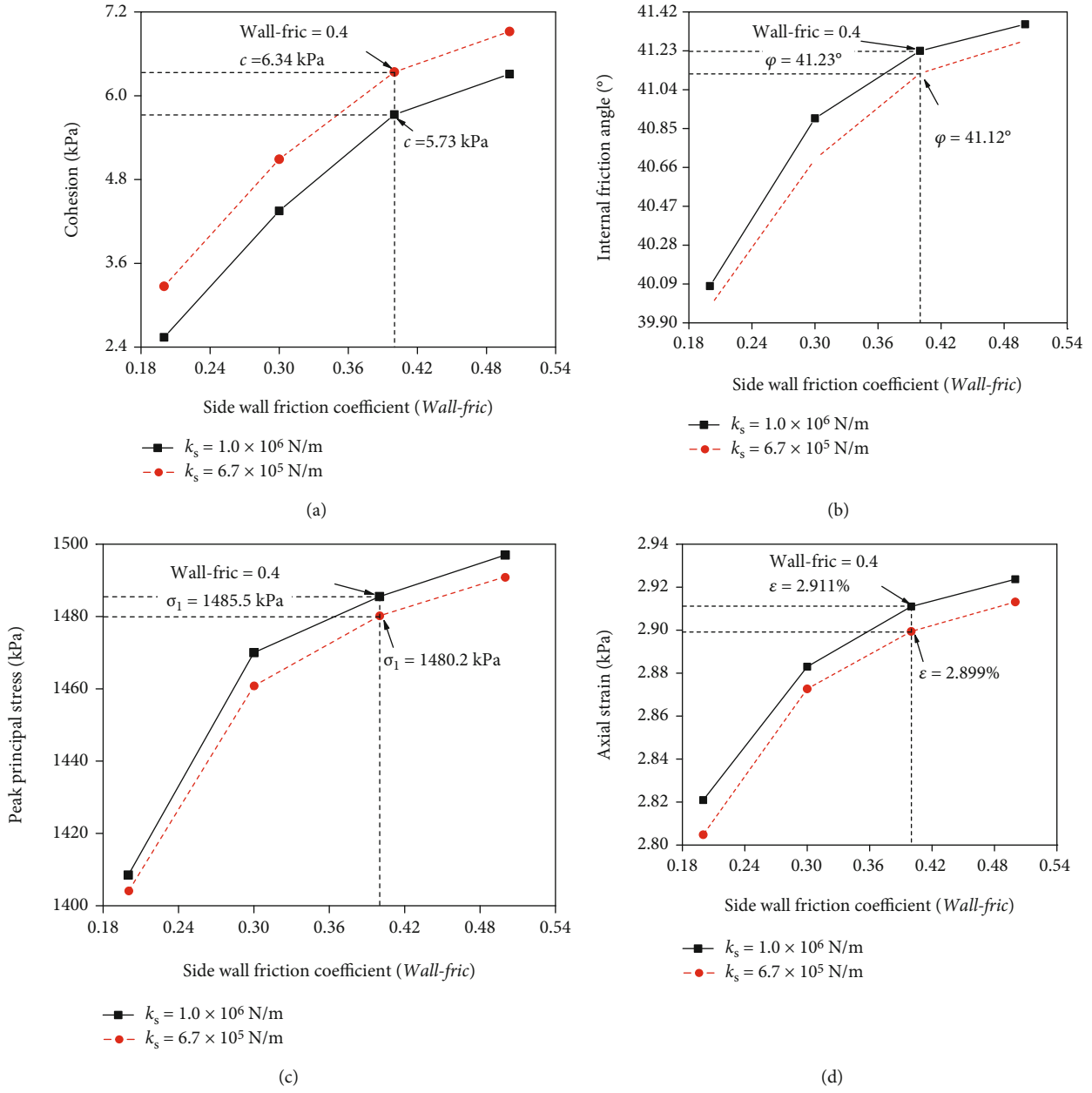
Figure 9: Influence of wall-fric on macromechanical parameters: (a) cohesion, (b) internal friction angle, (c) peak principal stress, and (d) axial strain.

Table 3: Rate of change of macromechanical parameters affected by changes in mesoparameters.

Macromechanical parameters	Mesoparameters			
	k_n	k_n/k_s	pebble-fric	wall-fric
Cohesion c	86.15% (4)	251.80% (1)	99.33% (3)	148.43% (2)
Internal friction angle φ	2.39% (4)	6.40% (2)	40.11% (1)	3.16% (3)
Peak principal stress	6.10% (3)	6.62% (2)	115.97% (1)	5.97% (4)
Peak corresponding strain	46.91% (1)	3.44% (3)	0.69% (4)	3.55% (2)

Note: the units in the table are the absolute values of the rate of change of each macroparameter. The values in parentheses represent the ranking of influence degree.
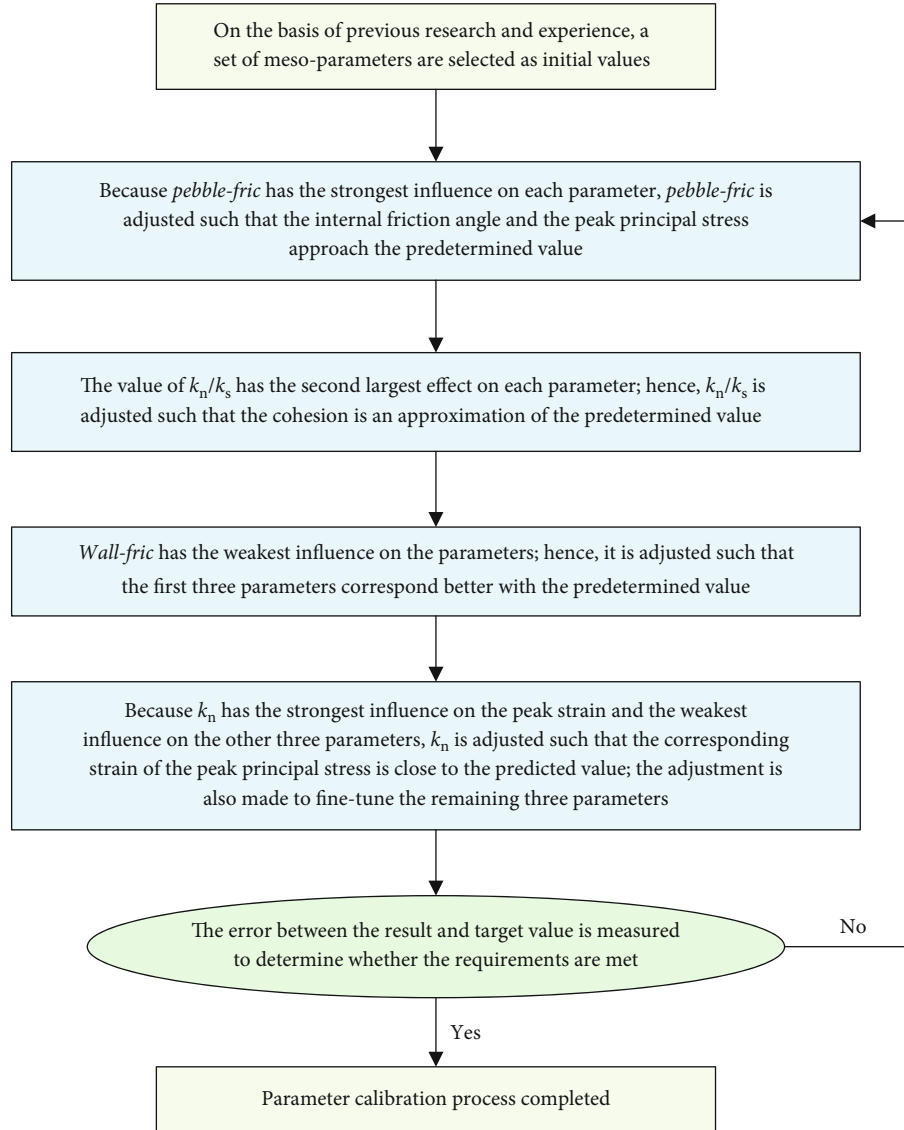
FIGURE 10: Calibration sequence process of mesoparameters of a linear contact model.

TABLE 4: Values of mesoparameters of tailing sand.

Category	k_n (N/m)	k_s (N/m)	fric	Density (kg/m^3)
Tailings	1.0×10^7	1.25×10^6	0.5	1,600

arbitrarily specified. As wall-fric increased, both cohesion and internal friction angle increased rapidly before the rate gradually slowed. The relationship curves under two conditions are parallel. With $k_s = 1.0 \times 10^6$ N/m, the cohesion increased from 2.54 kPa to 6.31 kPa, a total increase of 148.43%, and the internal friction angle increased from 40.08° to 41.36°, a total increase of 3.16%.

Figures 9(c) and 9(d) show that the peak principal stress and corresponding axial strain increased rapidly when wall-fric increased from 0.2 to 0.3, and the rate of increase substantially slowed down from 0.3 to 0.5. When $k_s = 1.0 \times 10^6$ N/m, the peak value of the principal stress increased from 1,408.5 kPa to 1,497.2 kPa, an increase of 5.97%, and

the axial strain increased from 2.82% to 2.92%, an increase of 3.55%.

5. Calibration Steps and Verification of Mesoparameters of Tailing Sand

In these experiments, the values of four mesoparameters were measured until the trend of change of macromechanical parameters considerably slowed down. The measurement was performed this way to aid the comparison of the parameter effect. Table 3 summarizes the rate of change of each macro-parameter affected by the change in each mesoparameter.

Table 3 presents the degree of influence on cohesion, demonstrating that $k_n/k_s >$ wall $-$ fric $>$ pebble $-$ fric $> k_n$. The degree of influence of the friction coefficient and contact stiffness of the fillers were approximately one-third of that of k_n/k_s, whereas the degree of influence of wall-fric was about half as large.
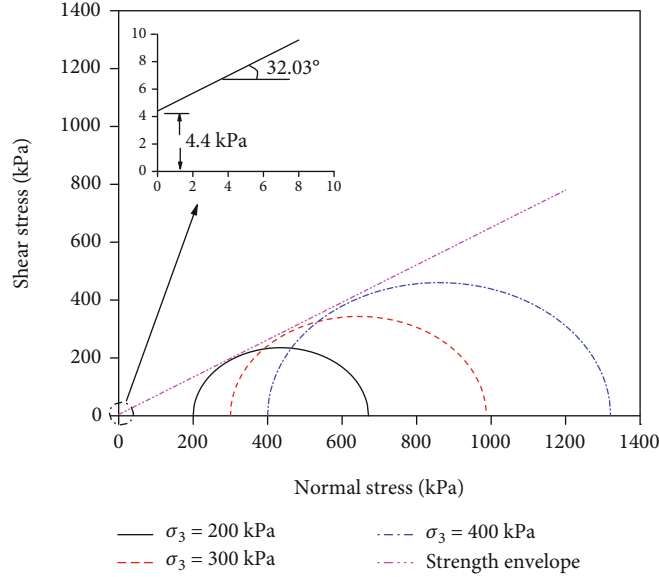
FIGURE 11: Numerical results under final parameters of tailing sand.

For the internal friction angle, the influence relationship was pebble – fric > k_n/k_s > wall – fric > k_n. The influence of pebble-fric was much higher than that of the other three mesoparameters, which were approximately one-sixth of the degree of influence.

Considering the effects of the mesoparameters on the peak principal stress, the relationship of the influence degree was approximately the same as that of the internal friction angle, but the influence of pebble-fric was approximately 17 times higher than that of other mesoparameters.

The influence degree of peak stress on strain was k_n > wall – fric > k_n/k_s > pebble – fric, where pebble-fric had almost no effect. The influence degree of wall-fric and k_n/k_s were similar, and the influence of k_n was more than 12 times as large.

The above results show that for each macroparameter, there is a single mesoparameter that has a much greater impact than the other three. Therefore, we should focus on adjusting specific mesoparameters during their selection, depending on the macroparameters of interest.

Considering the experimental results, we summarize in Figure 10 the process of selecting the mesoparameters for a PFC linear model.

After all the parameters are selected according to the process outlined above, the mesoparameters are fine-tuned to enhance the accuracy of the macromechanical characteristics. Table 3 and the corresponding analyses show that each mesoparameter has an influence on all macromechanical properties. Therefore, when choosing values for the mesoparameters, it is inadequate to only change the value of the main control mesoparameters with the aim of making the corresponding macromechanical parameters equal to the required values. Changes in other parameters must also be considered, which makes the selection of parameters faster. Parameter selection is a dynamic cyclic optimization process, and the results obtained in this study can provide a reli-

able basis for parameter adjustment and help to control the process dynamically.

Table 4 presents the final mesoparameters of tailing sand, which were obtained according to the correlation law of macro-mesoparameters, order of parameter adjustment, and preliminary adjustment.

The results of the numerical triaxial test are illustrated in Figure 11. The cohesion force of tailing sand adjusted by parameters was 4.4 kPa, and the internal friction angle was 32.03°. When the water content of the tailings was 12.4%, the errors between the interface strength parameters measured from the indoor triaxial test [20] were 6.38% and 2.61%, respectively.

6. Conclusion

(1) The nonspherical particles developed by the clump command can improve simulation accuracy as they are characterized by good spatial isotropy, which is crucial for the smooth transitioning of stress–strain curves and for overcoming the drawbacks of the overrotation of pure circular particles. Meanwhile, when the linear contact model is used to simulate sandy soil, the corresponding gradation should be applied to the particles for high consistency with the test results

(2) The mesoparameters of the linear contact model do not have single-factor effects on its macromechanical properties, but cross-effects exist. Each macromechanical parameter has a dominant controlling mesoparameter, which has a far greater impact than the other mesoparameters. The stiffness ratio (k_n/k_s) mainly affects the cohesion value, the friction coefficient of fillers (pebble-fric) mainly affects the internal friction angle and the peak principal stress, the

normal stiffness (k_n) of particles mainly affects the strain corresponding to the peak principal stress, and the influence of the friction coefficient of the side wall (wall-fric) is not the strongest but cannot be neglected

(3) In the process of calibrating mesoparameters of the linear contact model, the parameter adjustment should follow a certain order and consider cross-effects. The correlation between macro- and meso-parameters and the order of parameter adjustment was obtained experimentally and would facilitate the process of parameter calibration for linear contact model programs

Data Availability

The data used to support the findings of this study are included within the article.

Conflicts of Interest

The authors declare that there are no conflicts of interest regarding the publication of this paper.

Acknowledgments

References

[1] B. K. Mishra and C. V. Murty, "On the determination of contact parameters for realistic DEM simulations of ball mills," *Powder Technology*, vol. 115, no. 3, pp. 290–297, 2001.

[2] S. Masson and J. Martinez, "Effect of particle mechanical properties on silo flow and stresses from distinct element simulations," *Powder Technology*, vol. 109, no. 1-3, pp. 164–178, 2000.

[3] D. O. Potyondy and P. A. Cundall, "A bonded-particle model for rock," *International Journal of Rock Mechanics and Mining Sciences*, vol. 41, no. 8, pp. 1329–1364, 2004.

[4] J. M. M. Manuel and E. M. R. Luis, "Discrete numerical model for analysis of earth pressure balance tunnel excavation," *Journal of Geotechnical and Geoenvironmental Engineering*, vol. 131, no. 10, pp. 1234–1242, 2005.

[5] H. Landry, C. Lague, and M. Roberge, "Discrete element representation of manure products," *Computers and Electronics in Agriculture*, vol. 51, no. 1-2, pp. 17–34, 2006.

[6] Z. Asaf, D. Rubinstein, and I. Shmulevich, "Evaluation of link-track performances using DEM," *Journal of Terramechanics*, vol. 43, no. 2, pp. 141–161, 2006.

[7] H. Huang, B. Lecampion, and E. Detournay, "Discrete element modeling of tool-rock interaction I: rock cutting," *International Journal for Numerical and Analytical Methods in Geomechanics*, vol. 37, no. 13, pp. 1913–1929, 2013.

[8] W. Zhang, J. Q. Zou, K. Bian, and Y. Wu, "Thermodynamic-based cross-scale model for structural soil with emphasis on bond dissolution," *Canadian Geotechnical Journal*, vol. 59, no. 1, pp. 1–11, 2022.

[9] A. D. Renzo and F. Maio, "Comparison of contact-force models for the simulation of collisions in DEM- based granular flow codes," *Chemical Engineering Science*, vol. 59, no. 3, pp. 525–541, 2004.

[10] S. Hentz, L. Daudeville, and F. V. Donze, "Identification and validation of a discrete element model for concrete," *Journal of Eingineering Mechanics*, vol. 130, no. 6, pp. 709–719, 2004.

[11] B. Yang, J. Yue, and S. Lei, "A study on the effects of micro-parameters on macroproperties for specimens created by bonded particles," *Engineering Computations*, vol. 23, no. 6, pp. 607–631, 2006.

[12] J. Yoon, "Application of experimental design and optimization to PFC model calibration in uniaxial compression simulation," *International Journal of Rock Mechanics & Mining Sciences*, vol. 44, no. 6, pp. 871–889, 2007.

[13] Y. Cong, Z. Q. Wang, Y. R. Zheng, and X. T. Feng, "Experimental study on fine parameters of rock materials based on particle flow principle," *Geotechnical Journal*, vol. 37, no. 6, pp. 1031–1040, 2015.

[14] B. Zhou, H. B. Wang, W. F. Zhao, J. W. Li, and B. C. Zheng, "Correlation between fine and macroscopic mechanical parameters of cohesive materials," *Geotechnics*, vol. 33, no. 10, pp. 3171–3175+3177-3178, 2012.

[15] X. M. Xu, D. S. Ling, Y. M. Chen, and B. Huang, "Study on the correlation of fine-macroscopic elastic constants of granular materials based on linear contact model," *Journal of Geotechnical Engineering*, vol. 32, no. 7, pp. 991–998, 2010.

[16] X. Huang, K. J. Hanley, C. O'Sullivan, C. Y. Kwok, and M. A. Wadee, "DEM analysis of the influence of the intermediate stress ratio on the critical-state behaviour of granular materials," *Granular Matter*, vol. 16, no. 5, pp. 641–655, 2014.

[17] J. Zhou, Y. W. Chi, Y. Chi, and J. P. Xu, "Simulation of biaxial test on sand by particle flow code," *Chinese Journal of Geotechnical Engineering*, vol. 6, pp. 701–704, 2000.

[18] C. Chen, G. R. McDowell, and N. H. Thom, "Investigating geogrid-reinforced ballast: Experimental pull-out tests and discrete element modelling," *Soils and Foundations*, vol. 54, no. 1, pp. 1–11, 2014.

[19] J. F. Ferellec and G. R. McDowell, "Modelling of ballast–geogrid interaction using the discrete-element method," *Geosynthetics International*, vol. 19, no. 6, pp. 470–479, 2012.

[20] Z. H. Meng, "Study on the shear behavior of geogrid reinforced tailings sand," *Highway Engineering*, vol. 39, no. 1, pp. 250–255, 2014.